

Non-adiabatic corrections to a chiral charge pumping in topological nodal semimetals

Matej Badin ^{1,2,*}

¹SISSA – Scuola Internazionale Superiore di Studi Avanzati, Via Bonomea 265, 34136 Trieste, Italy

²Department of Experimental Physics, Faculty of Mathematics, Physics and Informatics,
Comenius University in Bratislava, Mlynská Dolina F2, 842 48 Bratislava, Slovakia

(Dated: May 31, 2022)

Studying many-body versions of Landau-Zener-like problem of non-interacting electrons in the Slater formalism for several $\mathbf{k} \cdot \mathbf{p}$ models representing Weyl and Dirac semimetals, we systematically include non-adiabatic corrections to a quantum limit of chiral charge pumping in these models. Our study shows that *relative homotopy invariant* [Sun, X. et al., Phys. Rev. Lett. **121**, 106402 (2018)] and *Euler class invariant* [Bouhon, A. et al., Nat. Phys. **16**, 1137–1143 (2020)] non-trivially manifest in the non-adiabatic corrections to the quantum limit of chiral charge pumping. These corrections could affect conductivity channels connected with the presence of chiral anomaly. Moreover, we show that for *non-symmorphic systems* this contribution is sensitive to the direction of the applied magnetic field suggesting that the conjectured direction-selective chiral anomaly in non-symmorphic systems [Bzdušek, T. et al., Nature **538**, 75–78 (2016)] could lead to a strongly anisotropic longitudinal magnetoresistance. The presented approach can be easily applied to other $\mathbf{k} \cdot \mathbf{p}$ or tight-binding models.

I. INTRODUCTION

The characteristic feature of Weyl semimetals [1, 2] is the chiral anomaly [3, 4], experimentally manifested by a decrease of resistance in the presence of parallel electric and magnetic fields [5–7, 9–13]. In the quantum limit of strong magnetic fields [14] (when only a chiral Landau level is occupied), the chiral anomaly of Weyl semimetals follows from the presence of chiral Landau levels (LLs) which connect the conduction bands to the valence bands. A pair of counter-propagating chiral Landau levels also appear in Dirac semimetals [1], where a similar signature in magnetoresistance is expected if the relaxation time of electrons is sufficiently large. Curiously, it has been reported that certain class of nodal-ring semimetals in non-symmorphic systems [15] should also exhibit chiral Landau levels, but only for special high-symmetry directions of the applied magnetic field.

In a Weyl semimetal, in the adiabatic limit (for sufficiently weak electric field), the motion of electrons can be modeled by the semi-classical approach [5–7], where the presence of chiral LL implies pumping of electrons from occupied to unoccupied bands at rate [5–7]

$$\frac{\partial Q}{\partial t} = -\chi V \frac{e^3}{4\pi^2 \hbar^2} \mathbf{E} \cdot \mathbf{B}, \quad (1)$$

where χ is the chirality of Weyl node, V is the volume of the sample and \mathbf{E} and \mathbf{B} are the electric and magnetic fields, respectively. Due to the Nielsen-Ninomiya theorem [8] the Weyl points can appear only in pairs of the opposite chiralities. In the semi-classical Boltzmann formalism, Son and Spivak [7] showed that the chiral charge pumping- Eq. (1) of two nodes possessing the opposite chiralities can be stabilized by an inter-node scattering of a finite relaxation time τ leading to a finite field-dependent contribution to a conductivity [7]

$$\sigma(B) = \frac{e^3}{2\pi^2 \hbar} B \tau. \quad (2)$$

In the quantum limit [14] (when only the chiral Landau level is occupied) and if the adiabatic approximation holds (for sufficiently weak electric fields) this formula is exact for every pair of Weyl nodes. Recently, the deviations from both limits have been studied in Refs. [14, 16].

In Ref. [14], Das *et al.* examined the case when multiple Landau levels become occupied as the cyclotron frequency (magnetic field) is lowered compared to the chemical potential (Fermi level). This lead to the quantum oscillations in longitudinal and planar transport coefficients which are periodic in $1/B$ [14].

Hwang *et al.* [16] consider a situation when the electric field is arbitrarily large leading to a general Landau-Stark resonance. They consider both Landau and Stark quantization of energy levels for a minimal model of tight-binding Weyl semimetal and then study nonequilibrium quantum transport on impurities using the Keldysh-Dyson formalism. They showed that their minimal tight-binding model does not allow a Landau-Zener transition between different LLs since the Berry connection is strictly zero (between different LLs). However, this does not need to be the case for other models of Weyl or Dirac semimetals, and hence a Landau-Zener transition can be allowed in other models.

Moreover, the usual semi-classical Boltzmann formalism or respectively the formula given by Eq. (1) become inapplicable if a Landau spectrum of a considered model shows occasional as well as symmetry-protected degeneracies (when adiabatic approximation can fail). For example, this is exactly the case for the so-called *non-symmorphic nodal loops* and *nodal chains* proposed in Ref. [15]. Therefore, a way able to incorporate non-adiabatic corrections into the calculation (of the chiral charge pumping) is sought.

This work is organized as follows. In Sec. II, we describe a simple numerical method that enables to include non-adiabatic corrections to the pumping rate given by Eq. (1) (or its analogues). Namely, we show how to calculate the expectation value of the number of electrons in the conduction bands still within the quantum limit but allowing for corrections implied by a finite value of electric field.

* mbadin@sissa.it

In Sec. III and Sec. IV, we show that simple models (“filling” the Nielsen-Ninomiya theorem [8]; thus possessing two Weyl nodes of the opposite chirality) that do and do not possess the *relative homotopy invariant* [17] or *Euler class invariant* [18] show a non-trivial signature in the mentioned non-adiabatic corrections to the chiral charge pumping possibly measurable in experiments. Namely, we show that the deviations from the expected values take place before the onset of annihilation of Weyl points (in respect to the model free parameters).

Finally, in Sec. V numerical results are presented for the class of Dirac semimetals possessing so-called *non-symorphic nodal loops* [15]. Curiously, a similar $1/B$ oscillation pattern is observed in the chiral charge pumping compared to the quantum oscillations in Ref. [14] even of completely different origin.

II. METHOD

We consider a simple many-body version of Landau-Zener-like problems of non-interacting electrons in $\mathbf{k} \cdot \mathbf{p}$ models under the presence of magnetic and electric fields. The first implies the presence of an infinite ladder of Landau levels (LLs), the later implies that we allow electrons to tunnel to neighboring LLs. We set Fermi level to zero energy, $\varepsilon_F = 0$, and consider the time-evolution of Slater determinants of momentum-dependent Hamiltonians under the presence of electric field. We consider only Slater determinants of electron states in which all electrons share the same value of momentum k_z .

The presence of the electric field is modelled semi-classically as

$$\partial_t k_z = -eE/\hbar, \quad (3)$$

meaning that the electrons move along the 1D bands opposite to the direction of \mathbf{E} . The semi-classical motion is immediately solved as $k_z(t) = -eEt/\hbar$. The presence of magnetic field is modelled by the standard Peierls substitution in the corresponding $\mathbf{k} \cdot \mathbf{p}$ model. The time evolution of the system is modelled in the quantum limit following the time-dependent Schrödinger equation (TDSE),

$$i\hbar\partial_t |\psi(k_z)\rangle = \mathcal{H}^{\text{many}}(k_z) |\psi(k_z)\rangle, \quad (4)$$

where $k_z(t) = -eEt/\hbar$ and $|\psi(k_z)\rangle$ is a many-electron wave function expressed in a basis of Slater determinants. The state $|\psi(k_z)\rangle$ is initially in the limit $t \rightarrow -\infty$ (replaced by a finite numerical value in numerical calculations) set to the state in which all LLs corresponding to the valence bands are completely filled.

Under the assumption of non-interacting electrons, the many-electron Hamiltonian $\mathcal{H}^{\text{many}}(k_z)$ is the antisymmetric part of a tensor product of the single particle Hamiltonians $\mathcal{H}(k_z)$. Hence, it follows that the time evolution of the many-body state $|\psi(k_z)\rangle$ can be expressed using the time evolution of eigenstates of (single-electron) $\mathcal{H}(k_z)$ only.

For every considered $\mathbf{k} \cdot \mathbf{p}$ model, we calculate the expectation value $N_{\text{ex}}(E, B)$ of number of electrons in the conductive

bands in the limit $t \rightarrow \infty$ (replaced by a finite value in numerical calculations). In the semi-classical limit, this expectation value enters the pumping rate through relation

$$\frac{\partial Q}{\partial t} = -\frac{N_{\text{ex}}(E, B)e^2 E}{\Delta k_z \hbar} N_{\text{deg}} = -N_{\text{ex}}(E, B) \frac{e^3 V}{4\pi^2 \hbar^2} EB, \quad (5)$$

where $N_{\text{deg}} = \phi/\phi_0 = BL_x L_y / (2\pi\hbar/e)$ is the degeneracy of LL, $\Delta k_z = 2\pi/L_z$ is the spacing of the available states in the k -representation, $V = L_x L_y L_z$ is the volume of a sample and L_x, L_y and L_z are linear dimensions of the sample.

Note that any choice of model under presence of magnetic field implies an infinite ladder of LLs below and above the Fermi level. Therefore, we limit ourselves to only N above and below it. The fermionic subspace of $\mathcal{H}^{\text{many}}$ has still the dimensionality of $S = \binom{2N}{N} > 2^N$. To avoid this scaling, we express the many-electron wave function in the basis of a limited number of Slater determinants created from the single-electron eigenstates $|\psi_n(k_z)\rangle$ of $\mathcal{H}(k_z)$.

We limit only to the Slater determinants containing up to M ($M < N$) electrons in the excited ($\varepsilon_n > 0$) single-particle states. That creates a basis of $S_M = \sum_{i=0}^M \binom{N}{i}^2 \sim N^M$ Slater determinants $|\varphi_i(k_z)\rangle$. The many-electron wave function $|\psi(k_z)\rangle$ is then expressed as

$$|\psi(k_z)\rangle = \sum_i^{S_M} c_i(k_z) |\varphi_i(k_z)\rangle, \quad (6)$$

where $|\varphi_i(k_z)\rangle$ is a Slater determinant of the form

$$|\varphi_i(k_z)\rangle = \frac{1}{\sqrt{N!}} \sum_{\tau} \text{sign } \tau \left(\bigotimes_j |\psi_{\tau(\alpha_i(j))}(k_z)\rangle \right), \quad (7)$$

in which $\text{sign } \tau = \pm 1$ is the parity of permutation τ and $\alpha_i(j)$ goes over the set of N one-electron eigenstates from which the Slater determinant is constructed.

Under the assumption of non-interacting electrons, the Slater determinant $|\varphi_i(k_z)\rangle$ is an eigenstate of $\mathcal{H}^{\text{many}}(k_z)$ with energy $\varepsilon_i(k_z) = \sum_{j=1}^N \varepsilon_{\alpha_i(j)}(k_z)$. It follows that the many-electron TDSE (Eq. (4)) (almost) diagonalizes in Slater formalism into the simple system of dimensionality S_M ,

$$i\hbar C_{ij}^{-1} \partial_t c_j(k_z) = \varepsilon_i(k_z) c_i(k_z), \quad (8)$$

where C_{ij} is the overlap matrix between the eigenstates of $\mathcal{H}^{\text{many}}(k_z + \Delta k)$ and the eigenstates of $\mathcal{H}^{\text{many}}(k_z)$.

The solution of Eq. (8) just requires to find a suitable time propagator $\mathcal{U}_{ij}(t + \Delta t, t)$ which under Eq. (3) can be written as $\mathcal{U}_{ij}(k_z - \Delta k, k_z)$.

The time evolution can than be expressed only as a problem of evolution of basis set coefficients and a simple matrix-vector equation given the suitable propagator $\mathcal{U}_{ij}(k_z - \Delta k, k_z)$ exists,

$$c_i(k_z - \Delta k) = \mathcal{U}_{ij}(k_z - \Delta k, k_z) c_j(k_z). \quad (9)$$

In this work we use a simple Euler forward propagator,

$$\begin{aligned} \mathcal{U}_{ij}(k_z - \Delta k, k_z) &= \sum_{n=0}^{S_M} \langle \varphi_i(k_z - \Delta k) | \varphi_n(k_z - \Delta k/2) \rangle \cdot \\ &\exp\left(\frac{i\Delta k_z}{E} \varepsilon_n(k_z - \Delta k/2)\right) \cdot \\ &\langle \varphi_n(k_z - \Delta k/2) | \varphi_j(k_z) \rangle. \end{aligned} \quad (10)$$

and achieve the unitarity of the time evolution by the normalisation of the wave function after every step.

Performing the real-time integration given by Eqs. (9) and (10) we are able to find the expectation value $N_{\text{ex}}(E, B)$ in the limit $t \rightarrow \infty$.

Since the dot product of two Slater determinants can be calculated in $\mathcal{O}(N^3)$ steps, see App. C, the evolution can be evaluated in $\mathcal{O}(S_M^2 N^3) \sim \mathcal{O}(N^{2M+3})$ steps.

The results of numerical algorithm are verified on a single-node isotropic Weyl point $\mathbf{k} \cdot \mathbf{p}$ model presented in App. A

III. RELATIVE HOMOTOPY INVARIANT

A. Models

In the presence of a mirror symmetry $m_z : (x, y, z) \mapsto (x, y, -z)$, a pair of mirror-related Weyl points (WPs) carry opposite chirality. While it is generally expected that such WPs pairwise annihilate at the symmetric plane upon collision, it has been reported [17] that a finer relative homotopy invariant may prevent their annihilation, enforcing instead their conversion into a nodal loop (NL). Such a scenario prominently arises for two-band models based on a pair of orbitals with different m_z eigenvalue [19], while a trivial annihilation occurs if the two orbitals have the same mirror eigenvalue.

We consider minimal $\mathbf{k} \cdot \mathbf{p}$ models belonging to both topological classes, assuming for simplicity an additional $\text{SO}(2)$ symmetry around the mirror normal. For the trivial case with mirror operator $\hat{m}_z = \mathbb{1}$, we take

$$\mathcal{H}_A(\mathbf{k}) = \hbar v (k_x \sigma_x + k_y \sigma_y) + (m - \alpha k_z^2) \sigma_z, \quad (11)$$

which for $m/\alpha > 0$ exhibits a pair of WPs at $(0, 0, \pm \sqrt{m/\alpha})$ that annihilate for $m = 0$ at $\mathbf{k} = \mathbf{0}$. For the non-trivial case with mirror operator $\hat{m}_z = \sigma_z$, the minimal model must include higher-order terms. We specifically take

$$\begin{aligned} \mathcal{H}_B(\mathbf{k}) &= \alpha k_z (k_x \sigma_x + k_y \sigma_y) \\ &+ (\beta (k_x^2 + k_y^2 - k_z^2) + m) \sigma_z, \end{aligned} \quad (12)$$

which [similar to $\mathcal{H}_A(\mathbf{k})$] for $m > 0$ exhibits a pair of WPs at $(0, 0, \pm \sqrt{m/\beta})$, that [as opposed to $\mathcal{H}_A(\mathbf{k})$] convert to a NL in $k_z = 0$ with radius $\kappa = \sqrt{-m/\beta}$ for $m/\beta < 0$. A two-band model similar to $\mathcal{H}_B(\mathbf{k})$ (but with twice the value of the relative homotopy invariant, and with a flipped sign of the $k_z^2 \sigma_z$ term) has been considered for ferromagnetic HgCr_2Se_4 [20]. The recent work [21] showed that the relative homotopy invariant of the band nodes in HgCr_2Se_4 is of a delicate topological character.

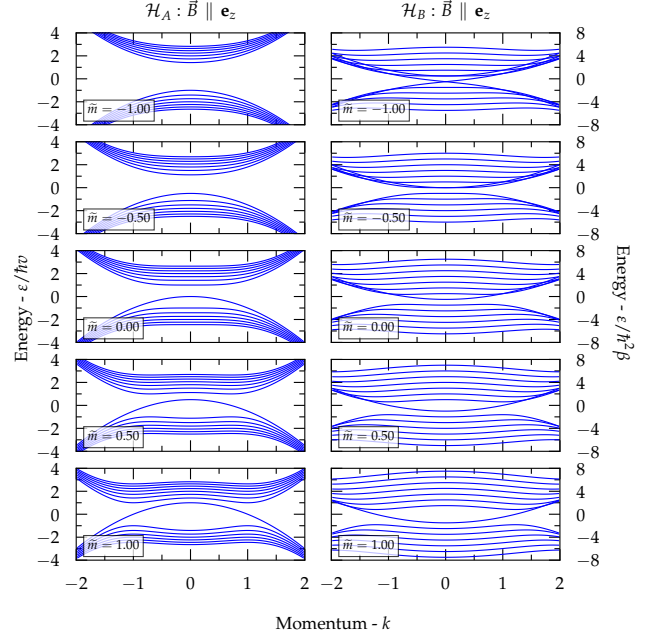


FIG. 1. LLs of $\mathcal{H}_A(\mathbf{k})$ and $\mathcal{H}_B(\mathbf{k})$ for the magnetic field oriented along the z -axis and $B = 0.5$ for various choices of \tilde{m} ($\tilde{m} = m/\hbar v$ for $\mathcal{H}_A(\mathbf{k})$ and $\tilde{m} = m/\hbar^2\beta$ for $\mathcal{H}_B(\mathbf{k})$). Note the pair of WPs for $\tilde{m} > 0$ for $\mathcal{H}_A(\mathbf{k})$ and the manifestation of the NL as a point in this orientation of magnetic field for $\mathcal{H}_B(\mathbf{k})$ and $\tilde{m} < 0$. Seven LLs below and above the Fermi level are shown.

A slightly adjusted version of $\mathcal{H}_A(\mathbf{k})$ also governs the conversion of WPs into NL in ZrTe , where the parameter m is manipulated by strain [18]; here, the topological stability is enhanced by a $C_2\mathcal{T}$ -protected non-Abelian topological invariant [22].

LLs of the models are presented in Figs. 1 and 2. In the numerical calculation we set the values of $\hbar v = \alpha = 1$ for $\mathcal{H}_A(\mathbf{k})$ and $\alpha = \hbar^2\beta = 1$ for $\mathcal{H}_B(\mathbf{k})$.

B. Pumping rate

In Fig. 3 we show the expectation value of excited electrons in the conductive bands - $N_{\text{ex}}(E, B)$ (or to be more precise - $N_{\text{ex}}(\tilde{E}, \tilde{B})$, where \tilde{E} and \tilde{B} are rescaled fluxes of electric and magnetic fields E and B (to be defined later), respectively) - modifying the quantum limit of charge pumping created by the presence of chiral anomaly.

While the model $\mathcal{H}_A(\mathbf{k})$ without the additional $\text{SO}(2)$ symmetry around the mirror normal does not show any significant additional structure in $N_{\text{ex}}(\tilde{E}, \tilde{B})$, see Fig. 1(a), the model $\mathcal{H}_B(\mathbf{k})$ possessing nontrivial $\text{SO}(2)$ symmetry shows an additional structure for $\vec{B} \parallel \mathbf{e}_z$ and $m < 0$, see the stripes at Fig. 3(b). This structure is caused by gap closings at specific values of \tilde{m} , e.g., $\tilde{m} = -1$, see Fig. 1. These periodic-in- \tilde{m} gap closings are related to the gapless band structure of the nodal-loop phase and are protected by the mirror symmetry.

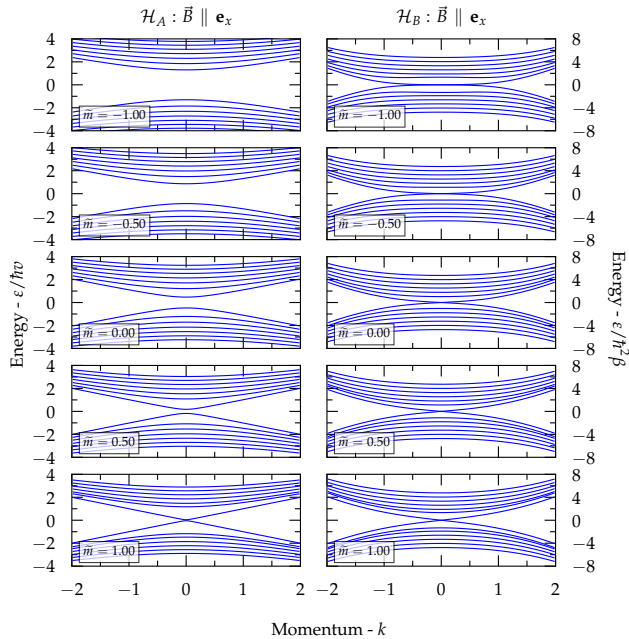


FIG. 2. LLs of $\mathcal{H}_A(\mathbf{k})$ and $\mathcal{H}_B(\mathbf{k})$ for the magnetic field oriented along the x -axis and $\vec{B} = 0.5$ for various choices of \tilde{m} ($\tilde{m} = m/\hbar v$ for $\mathcal{H}_A(\mathbf{k})$ and $\tilde{m} = m/\hbar^2\beta$ for $\mathcal{H}_B(\mathbf{k})$). Note the NL for $\tilde{m} < 0$ and $\mathcal{H}_B(\mathbf{k})$. Seven LLs below and above the Fermi level are shown.

However, if one is given a WSM phase with two Weyl points that approach one another after tuning some parameter (e.g., \tilde{m}), then the \tilde{m} -dependence of the pumping rate in applied $\vec{B} \parallel \mathbf{e}_z$ does not reveal whether the Weyl points would annihilate or convert into the NL semimetal: we find that the dependence on the WSM side of the phase diagram (of $N_{\text{ex}}(\vec{E}, \vec{B})$) is qualitatively the same for both $\mathcal{H}_A(\mathbf{k})$ and $\mathcal{H}_B(\mathbf{k})$, except the occasional gap closing at specific values of \tilde{m} .

The models can be easily distinguished if $\vec{B} \parallel \mathbf{e}_x$, where both models show different structure of $N_{\text{ex}}(\vec{E}, \vec{B})$ in respect to the parameter \tilde{m} , see Fig. 3(c-d).

Namely, observe that the pumping rate for the Hamiltonian $\mathcal{H}_B(\mathbf{k})$ with non-trivial relative homotopy invariant is *de facto* constant as a function of \tilde{m} . In contrast, for $\mathcal{H}_A(\mathbf{k})$, where the Weyl points are able to annihilate, we observe a decrease in pumping rate *before* the Weyl points actually annihilate. This early vanishing of the chiral anomaly is particularly pronounced for small values of \vec{E}/\vec{B} (i.e., weak electric field or strong magnetic field). This can be easily explained by the occurrence of degenerate WP for $\mathcal{H}_A(\mathbf{k})$ while for $\mathcal{H}_B(\mathbf{k})$ NL or WP is always present in respect to \tilde{m} , see Fig. 2.

Furthermore, for sufficiently high values of \tilde{m} , $\mathcal{H}_A(\mathbf{k})$ and $\vec{B} \parallel \mathbf{e}_z$, an interference pattern can be observed on $N_{\text{ex}}(\vec{E}, \vec{B})$, see Fig. 3(a). It corresponds to the presence of top-most valence band close to the conductive bands at $k = 0$, see Fig. 1 - the region around $\tilde{m} = 1$. The precise value of \tilde{m} for such a constructive/destructive interference appears is determined by the time the electron in the top-most valence band spends in a

vicinity of the conduction bands.

For the calculation of $N_{\text{ex}}(\vec{E}, \vec{B})$, see Fig. 3, in each of two bands 7 LLs were considered leading to overall 13 LLs (after removing a ghost state). Slater determinants with up to $M = 2$ excited electrons (implying overall 469 Slater determinants) were used and overall 1402 k -points were used in the simulation of real-time dynamics. Note that for the proper identification of ghost states, the matrix representations of $\mathcal{H}_A(\mathbf{k})$ and $\mathcal{H}_B(\mathbf{k})$ are truncated at a much higher number of states (80) than just the number of considered LLs (13).

IV. EULER CLASS INVARIANT

A. Models

It is known that $C_{2z}\mathcal{T}$ symmetry (composition of time reversal with π rotation around the z axis) can stabilize Weyl points inside a symmetric plane $k_z = 0$ (or $k_z = \pi$), as observed e.g. in the $k_z = 0$ plane of WTe₂ [23], MoP [24] and TaAs [25–27]. Besides their chiral charge, such WPs are also characterized by their Euler class invariant [18]. A non-trivial value of the Euler class prevents pairwise annihilation of colliding WPs with the same chirality inside the symmetric plane.

We consider minimal $C_{2z}\mathcal{T}$ -symmetric $\mathbf{k} \cdot \mathbf{p}$ models that describe a pair of colliding WPs with opposite chirality with trivial vs. non-trivial Euler class. For the trivial case, we consider

$$\mathcal{H}_C(\mathbf{k}) = 2(\alpha k_x k_y - m)\sigma_x + \hbar v(k_z \sigma_y + (k_x - k_y)\sigma_z), \quad (13)$$

which for $m/\alpha > 0$ exhibits a pair of WPs of opposite chirality at $\pm(\sqrt{m/\alpha}, \sqrt{m/\alpha}, 0)$ that annihilate for $m = 0$ at $\mathbf{k} = \mathbf{0}$. We contrast this to a model with a non-trivial value of the Euler class, namely

$$\mathcal{H}_D(\mathbf{k}) = 2(\alpha k_x k_y - m)\sigma_x + \beta k_x k_z \sigma_y + \gamma(k_x^2 - k_y^2 - k_z^2)\sigma_z, \quad (14)$$

which [similar to $\mathcal{H}_C(\mathbf{k})$] for $m/\alpha > 0$ exhibits a pair of WPs of opposite chirality at $\pm(\sqrt{m/\alpha}, \sqrt{m/\alpha}, 0)$, that [as opposed to $\mathcal{H}_C(\mathbf{k})$] collide at $\mathbf{k} = \mathbf{0}$ and bounce to form WPs at $\pm(\sqrt{-m/\alpha}, -\sqrt{-m/\alpha}, 0)$ for $m < 0$. While we are unaware of material examples exhibiting Weyl points that scatter after collision due to non-trivial of the Euler class, they could potentially be implemented and probed in cold-atom setups [28].

LLs of the models are presented in Figs. 4 and 5. In the numerical calculation we set the values of $\hbar v = \alpha = 1$ for $\mathcal{H}_C(\mathbf{k})$ and $\alpha = \beta = \gamma = 1$ for $\mathcal{H}_D(\mathbf{k})$.

B. Pumping rate

In Fig. 6 we show the expectation value of excited electrons in the conductive bands - $N_{\text{ex}}(\vec{E}, \vec{B})$ - modifying the chiral charge pumping for models of trivial ($\mathcal{H}_C(\mathbf{k})$) and nontrivial ($\mathcal{H}_D(\mathbf{k})$) Euler class.

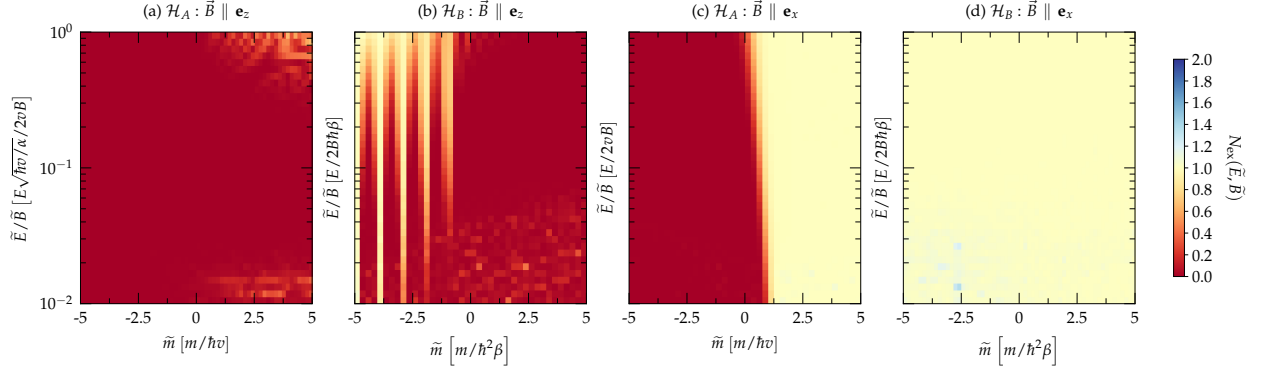


FIG. 3. Panels (a) - (d) - The expectation value $N_{\text{ex}}(\tilde{E}, \tilde{B})$ of number of electrons in the conductive bands as a function of the ratio of rescaled magnetic and electric fields - \tilde{E}/\tilde{B} and the rescaled parameter \tilde{m} for the various orientations of magnetic field.

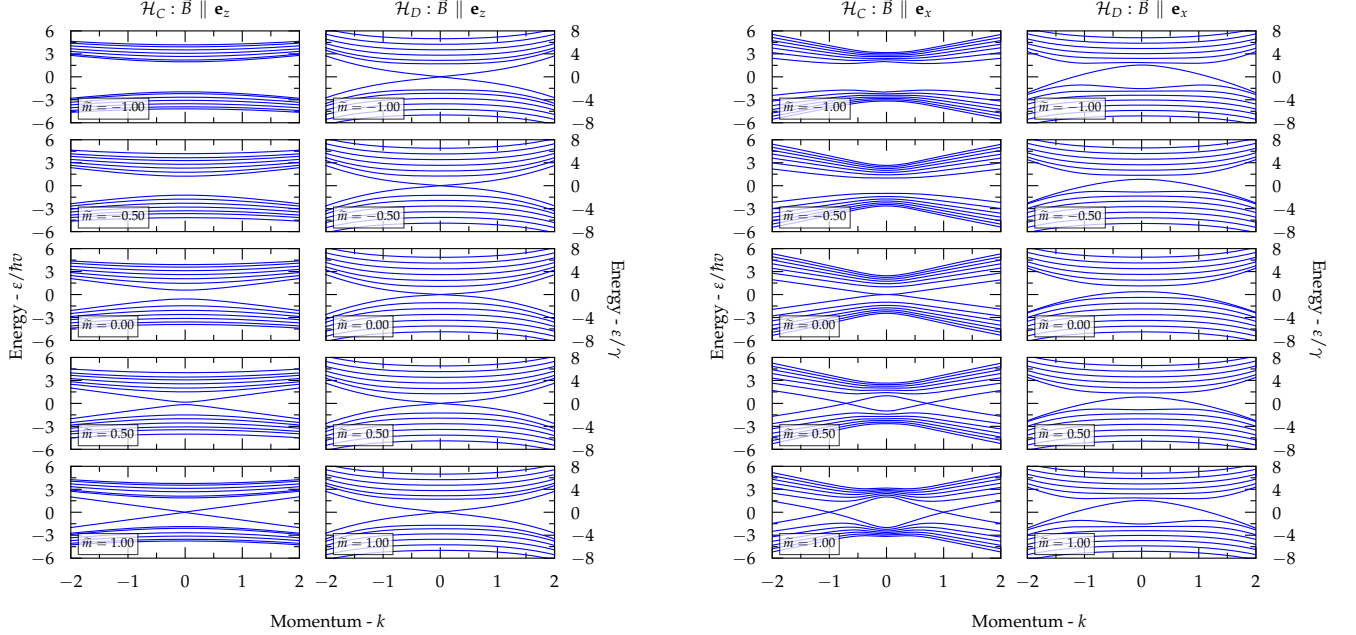


FIG. 4. LLs of $\mathcal{H}_C(\mathbf{k})$ and $\mathcal{H}_D(\mathbf{k})$ for the magnetic field oriented along the z-axis and $B = 0.5$ for various choices of \tilde{m} ($\tilde{m} = m/hv$ for $\mathcal{H}_C(\mathbf{k})$ and $\tilde{m} = m/\gamma$ for $\mathcal{H}_D(\mathbf{k})$). Seven LLs below and above the Fermi level are shown.

The models can be easily distinguished by the application of the magnetic field along any direction. If $\tilde{B} \parallel \mathbf{e}_z$, the non-trivial model ($\mathcal{H}_D(\mathbf{k})$) does not show any deviation from the value $N_{\text{ex}}(\tilde{E}, \tilde{B}) = 1$ while the trivial one ($\mathcal{H}_C(\mathbf{k})$) differs in respect to the sign of \tilde{m} . This behavior can be easily explained via the corresponding LLs.

For the trivial model, the deviation from the value $N_{\text{ex}}(\tilde{E}, \tilde{B}) = 1$ is caused by the gap opening (annihilation of

FIG. 5. LLs of $\mathcal{H}_C(\mathbf{k})$ and $\mathcal{H}_D(\mathbf{k})$ for the magnetic field oriented along the x-axis and $B = 0.5$ for various choices of \tilde{m} ($\tilde{m} = m/hv$ for $\mathcal{H}_C(\mathbf{k})$ and $\tilde{m} = m/\gamma$ for $\mathcal{H}_D(\mathbf{k})$). Seven LLs below and above the Fermi level are shown.

WP), see Fig. 4, as one decreases \tilde{m} . On the contrary for non-trivial model the WP is presented for any value of \tilde{m} , see Fig. 4. Namely, observe that the pumping rate for the Hamiltonian $\mathcal{H}_C(\mathbf{k})$ with trivial Euler class the hybridization of chiral LLs upon the change of parameter \tilde{m} is pronounced for small values of \tilde{E}/\tilde{B} (i.e., weak electric field, strong magnetic field) before the Weyl points annihilate. Therefore, a decline of $N_{\text{ex}}(\tilde{E}, \tilde{B})$ from the expected limit - 1 (in here chosen units)

suggests trivial class.

More interestingly, the models show nontrivial behavior when the field if $\vec{B} \parallel \mathbf{e}_x$. The spectrum of the nontrivial model ($\mathcal{H}_D(\mathbf{k})$) is symmetric with respect to the \tilde{m} , see Fig. 5, which manifests itself in the $N_{\text{ex}}(\vec{E}, \vec{B})$ as the function of \tilde{m} , see Fig. 6(d). Note that a cusp visible at Fig. 6(d) disappears for the ratio $\vec{E}/\vec{B} > 1$, if one overcomes the critical value of \vec{E} which enables tunneling also for $\tilde{m} = 0$. The phase diagram of $N_{\text{ex}}(\vec{E}, \vec{B})$ for $\mathcal{H}_C(\mathbf{k})$, see Fig. 6(c), reveals a nontrivial structure - oscillations of $N_{\text{ex}}(\vec{E}, \vec{B})$ in respect to \tilde{m} which are caused by an interference. The precise value of \tilde{m} for such constructive/destructive interference to happen is determined by the time the electron in the top-most valence band spends in a vicinity of the conduction bands, see LLs in Fig. 5.

For the calculation of $N_{\text{ex}}(\vec{E}, \vec{B})$, see Fig. 6 the simulation parameters were the same as for the production of Fig. 3.

V. NON-SYMMORPHIC NODAL LOOPS

A. Model

In this section, we revisit the chiral Landau levels of nodal loops protected on the boundary of the Brillouin zone by a glide symmetry [15]. The elementary model of a non-symmorphic nodal loop (NSNL) is

$$\mathcal{H}_{\text{NSNL}}(\mathbf{k}) = \hbar v (k_x \Gamma_1 + k_y \Gamma_2 + k_z \Gamma_3) + w \Gamma_{34} \quad (15)$$

where $\{\Gamma_i\}_{i=1}^5$ are pairwise anticommuting Dirac matrices squaring to $+\mathbf{1}$, and $\Gamma_{ij} = -\frac{i}{2}[\Gamma_i, \Gamma_j]$. NSNLs can be obtained from a parent Dirac node in a \mathcal{PT} -symmetric crystal with screw rotation symmetry [29, 30] upon breaking the inversion symmetry. It has been argued by the original theoretical work on these systems [15] that NSNL exhibit Landau level crossing at zero energy for magnetic fields \mathbf{B} applied within the glide plane. Nevertheless, the chiral Landau levels are gapped if \mathbf{B} deviates from the high-symmetry plane. It has therefore been suggested that these models should exhibit a direction-selective chiral anomaly [15].

Here we use the method presented in Sec. II to investigate the disappearance of the chiral-anomalous pumping rate of the Hamiltonian in Eq. (15).

In Fig. 7 we show the band gap in LLs for $\mathbf{k} = 0$ as a function of applied magnetic field and the angle θ between the direction of the applied magnetic field and the plane of NSNL in k -space. LLs of the model as a function of the angle θ between the direction of the applied magnetic field and the plane of NSNL in k -space are presented in App. D in Figs. 11 - 13.

B. Pumping rate

In Fig. 8 we show the expectation value $N_{\text{ex}}(\vec{E}, \vec{B})$ as a function of the \vec{E}, \vec{B} and the angle θ between the direction of the applied magnetic field and the plane of NSNL in k -space. The

expected $N_{\text{ex}}(\vec{E}, \vec{B})$ for smaller values of \vec{E} are presented in Fig. 9.

Results show that $N_{\text{ex}}(\vec{E}, \vec{B})$ is highly sensitive to the direction of the applied magnetic field (the angle θ) and pronounced for small values of \vec{E} and \vec{B} (i.e., weak electric and magnetic fields). The *ladder of gap closing*, see Fig. 7, manifests in $N_{\text{ex}}(\vec{E}, \vec{B})$, see Fig. 9.

At $\theta = 90^\circ$ (the direction of the applied magnetic fields is perpendicular to the NSNL) the gap closes at $\vec{B} = 1/n$ (in chosen units), for $n \in \mathbb{N}$. For $\theta < 90^\circ$ this *ladder of gap closing* is shifted towards weaker magnetic fields, see Fig. 7 and is observable only with sufficiently weak electric fields too, see Fig. 9.

In the limit $\theta \rightarrow 0$, the *ladder structure* is completely suppressed by the presence of NSNL, see LLs in Fig. 11 in App. D and Fig. 7. In $N_{\text{ex}}(\vec{E}, \vec{B})$, the value 1 is exactly recovered which is changed only to higher values upon application of stronger electric fields. The critical value of electric field \vec{E} to which this *ladder of gap closing* is observable is strongly dependent on the angle θ too, see Fig. 9.

For sufficiently low value of magnetic field \vec{B} the gap is small and the NL is present, see spectra in App. D. The length of the NSNL in the k -space is proportional to $\cos(\theta)$. The length of NL affects the maximal values of \vec{E} , see Fig. 9, where the non-trivial behavior is observable.

For the calculation of $N_{\text{ex}}(\vec{E}, \vec{B})$, see Fig. 8, in each of four bands of $\mathcal{H}_{\text{NSNL}}$ 5 LLs were considered leading to $N = 9$ (after removing two ghost states). Slater determinants with up to $M = 2$ excited electrons (implying overall 1378 Slater determinants). 270 k -points were used in the simulation of real-time dynamics. The region approaching di-adiabatic limit ($\vec{E} > \vec{B}$) was omitted since it cannot be studied reasonably with this value of M . Note that for the proper identification of ghost states, the matrix representation of $\mathcal{H}_{\text{NSNL}}$ is truncated at a much higher number (160) than just the number of considered LLs (18).

VI. CONCLUSION

We demonstrated a simple numerical algorithm which allows for systematic inclusion of non-adiabatic contributions to the quantum limit of chiral charge pumping (still close to the sufficiently weak electric fields). Considering Landau-Zener-like problems and non-interacting many-body $\mathbf{k} \cdot \mathbf{p}$ models, we showed that in this non-adiabatic corrections to the quantum limit of the chiral charge pumping the *relative homotopy invariant* [17] and *Euler class invariant* [18] are non-trivially manifested. Moreover, this manifestation take place before the onsets of annihilation of Weyl points in respect to the model free parameters, suggesting that if it is this non-adiabatic contribution measurable, it could act as an experimental probe for the mentioned topological invariants. Furthermore, for *non-symmorphic systems* [15] we showed this contribution to be highly sensitive to the direction of the applied magnetic field. It is possible that this contribution is measurable in longitudinal magnetoresistance, if it is not su-

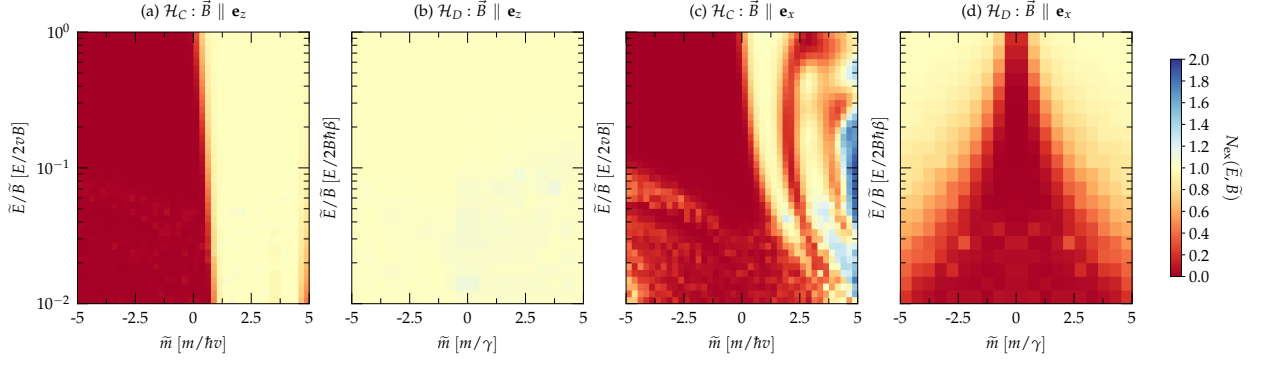


FIG. 6. Panels (a) - (d) - The expectation value $N_{\text{ex}}(\tilde{E}, \tilde{B})$ of number of electrons in conductive bands as a function of the ratio of rescaled magnetic and electric field - \tilde{E}/\tilde{B} and the rescaled parameter \tilde{m} for various orientations of magnetic field.

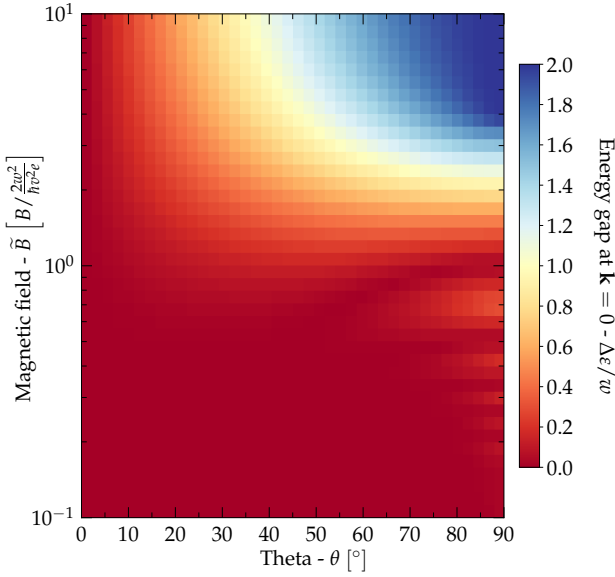


FIG. 7. Energy gap - $\Delta\varepsilon/w$ of $\mathcal{H}_{\text{NSNL}}(\mathbf{k})$ at $\mathbf{k} = 0$ as a function of the magnitude of the applied magnetic field \tilde{B} and the angle θ between the direction of the applied magnetic field and NSNL. Note the *ladder of gap closing* at $\theta = 90^\circ$ and $\tilde{B} = 1/n$ for $n \in \mathbb{N}$; which manifests in $N_{\text{ex}}(\tilde{E}, \tilde{B})$, see also Fig. 9.

pressed by other channels of conductivity in a particular material realisation. The presented approach can be easily applied to other $\mathbf{k} \cdot \mathbf{p}$ (e.g., double Dirac semimetals [31]) or tight-binding models.

ACKNOWLEDGMENTS

M.B. acknowledges stimulating discussions with T. Bzdušek and A. Soluyanov. M.B. was supported by Comenius University under Grant for Young Researchers No. UK/436/2021 and UK/454/2022, and by SAIA under National Scholarship Programme of the Slovak Republic in 2018. Calculations were performed on SISSA Ulysses and ETH Euler clusters.

Appendix A: Verification of the method on the single-node isotropic Weyl point model

To verificate the correctness of numerical calculations (the value - $N_{\text{ex}}(E, B)$) we apply the method to a single-node (isotropic) WP model adapted from Ref. [5]. We do not aim to make any conclusion here about the non-adiabatic contributions to the chiral charge anomaly in respect to the transport as a model of at least of two Weyl nodes of opposite chiralities would be needed, rather we want demonstrate the correctness of the numerical results for a simple model when Landau-Zener transition can be inferred analytically.

We consider the ideal Weyl Hamiltonian as

$$\mathcal{H} = \hbar v \mathbf{k} \cdot \boldsymbol{\sigma}, \quad (\text{A1})$$

where $\boldsymbol{\sigma} = (\sigma_x, \sigma_y, \sigma_z)$ are standard anticommuting 2×2 Pauli matrices, v has dimension of velocity, and \mathbf{k} is the momentum. The energy spectrum of this Hamiltonian is $\varepsilon_{\pm}(\mathbf{k}) = \pm \hbar v k$. Considering the ideal Weyl Hamiltonian in parallel magnetic and electric fields we can model the presence of a magnetic field by performing the Peierls substitution. We assume electric and magnetic fields to be

$$\mathbf{B} = (0, 0, B) \quad \text{and} \quad \mathbf{E} = (0, 0, E). \quad (\text{A2})$$

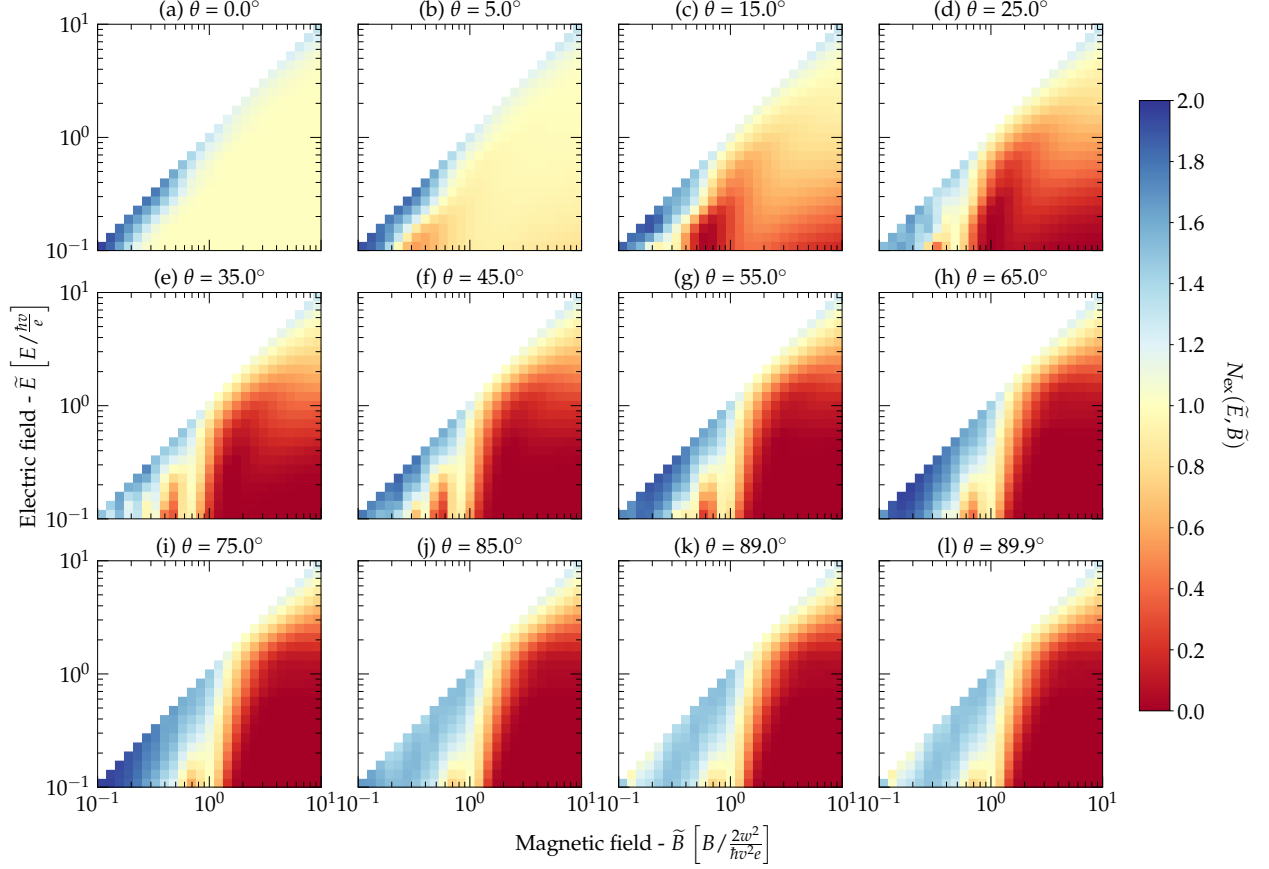


FIG. 8. The expectation value $N_{\text{ex}}(\tilde{E}, \tilde{B})$ of number of electrons in the conductive bands as a function of rescaled magnetic and electric fields - \tilde{B} and \tilde{E} . Panels (a) - (l) show disappearance of chiral-anomalous pumping if the direction of magnetic field deviates from the plane of NSNL in the region $\tilde{B} > 1$. In Fig. 9, we present details of phase diagrams for $\tilde{B} < 1$.

The Peierls substitution changes the operators of momentum,

$$\begin{aligned} (\hbar k_x, \hbar k_y, \hbar k_z) &\mapsto (-i\hbar\partial_x + eA_x, -i\hbar\partial_y + eA_y, \hbar k_z) \\ &\equiv (\Pi_x, \Pi_y, \hbar k_z), \end{aligned} \quad (\text{A3})$$

and the canonical momentum commutator changes to

$$[\Pi_x, \Pi_y] = ie\hbar(\partial_y A_x - \partial_x A_y) = -ie\hbar B. \quad (\text{A4})$$

Hence, the Π -operators can be expressed using the usual ladder operators $[a, a^\dagger] = 1$ as

$$\begin{aligned} \Pi_x &= \sqrt{\frac{e\hbar|B|}{2}}(a + a^\dagger) \\ \Pi_y &= i\text{sign}(B)\sqrt{\frac{e\hbar|B|}{2}}(a - a^\dagger). \end{aligned} \quad (\text{A5})$$

Assuming $B > 0$, the ideal Weyl Hamiltonian is changed into

$$\mathcal{H}(k_z) = v \begin{pmatrix} \hbar k_z & \sqrt{2e\hbar B}a \\ \sqrt{2e\hbar B}a^\dagger & -\hbar k_z \end{pmatrix}. \quad (\text{A6})$$

The corresponding energy spectrum is

$$\varepsilon_0(k_z) = -v\hbar k_z$$

$$\forall n \in \mathbb{Z} \setminus \{0\} : \varepsilon_n(k_z) = \text{sign}(n)v\sqrt{\hbar^2 k_z^2 + 2e\hbar B|n|}. \quad (\text{A7})$$

We define rescaled fluxes of electric and magnetic fields and expressed energy in multiples of $\hbar v$,

$$\tilde{E} = eE/\hbar v, \quad \tilde{B} = 2eB/\hbar, \quad \text{and} \quad \tilde{\varepsilon} = \varepsilon/(\hbar v). \quad (\text{A8})$$

In this convention, $\mathcal{H}(k_z)$ takes the form

$$\tilde{\mathcal{H}}(k_z) = \begin{pmatrix} k_z & \sqrt{\tilde{B}}a \\ \sqrt{\tilde{B}}a^\dagger & -k_z \end{pmatrix}, \quad (\text{A9})$$

and the TDSE takes form

$$i\partial_{k_z} |\psi(k_z)\rangle = -1/\tilde{E}\tilde{\mathcal{H}}(k_z)|\psi(k_z)\rangle. \quad (\text{A10})$$

Results of our method for this simple model are presented in Fig. 10. The diagram shows that for the Hamiltonian given

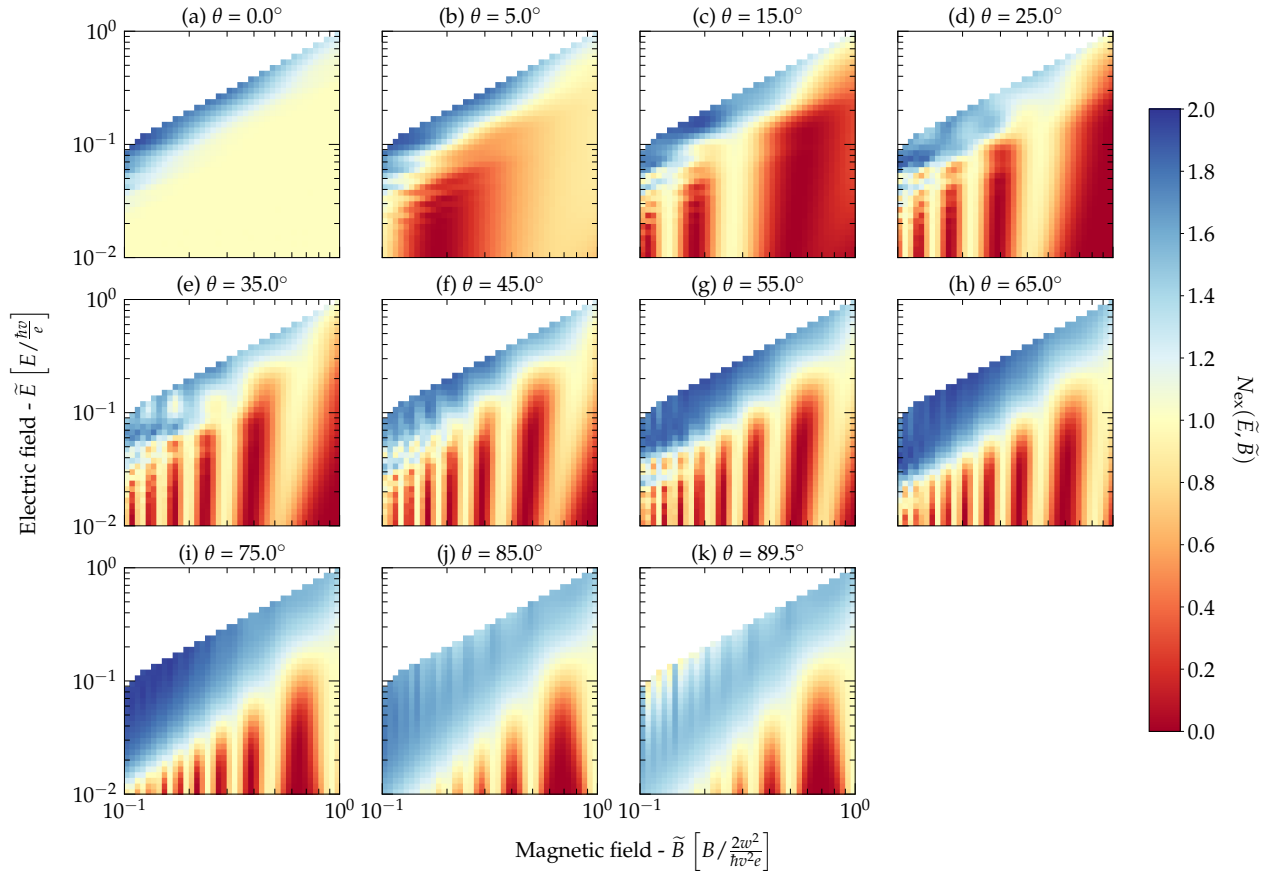


FIG. 9. The expectation value $N_{\text{ex}}(\tilde{E}, \tilde{B})$ of number of electrons in the conductive bands as a function of rescaled magnetic and electric fields - \tilde{B} and \tilde{E} in the region $\tilde{B} < 1$. All parameters of simulations are the same as for the phase diagrams presented in Fig. 8. Panels (a) - (b) show disappearance of chiral-anomalous pumping if the direction of magnetic field without any additional structure. Panels (c) - (k) reveal additional structures on disappearance of anomalous-chiral pumping due to gap closing of $\mathcal{H}_{\text{NSNL}}$ at certain values of magnetic field. Note that this "ladder" structure shifts towards smaller \tilde{B} with increasing the deviation (the angle θ) of applied magnetic field from the NSNL plane.

by Eq. (A1) the expectation value of $N_{\text{ex}}(\tilde{E}, \tilde{B})$ depends on \tilde{B} and \tilde{E} only via their ratio - \tilde{E}/\tilde{B} as heuristically argued in App. B. Note also a numerical noise visible in Fig. 10 in $N_{\text{ex}}(\tilde{E}, \tilde{B})$ in the region with $\tilde{E} < 10^{-2}$ where the used step Δk becomes inappropriate. The value of Δk were kept constant in all calculations presented in the phase diagram.

Appendix B: Heuristic argument for the dependence on the ratio - \tilde{B}/\tilde{E} only in isotropic WSM

The single-electron TDSE given in Eq. (A10) can be formally mapped to the class of Hamiltonians studied by Brundobler and Elser [32] (to the generalization of Landau-Zener

problem). The corresponding TDSE in their notation becomes

$$\begin{aligned} \mathcal{H}(t) &= \mathcal{A} + \mathcal{B}t, \\ i\partial_t \psi(t) &= \mathcal{H}(t)\psi(t), \end{aligned} \quad (\text{B1})$$

where \mathcal{A} and \mathcal{B} are constant Hermitian matrices. The identification is done as follows,

$$\begin{aligned} t &\rightarrow k_z, \\ \mathcal{A} &\rightarrow \begin{pmatrix} 0 & -\sqrt{\tilde{B}/\tilde{E}}\alpha \\ -\sqrt{\tilde{B}/\tilde{E}}\alpha^\dagger & 0 \end{pmatrix}, \\ \mathcal{B} &\rightarrow \begin{pmatrix} -1/\tilde{E} & 0 \\ 0 & 1/\tilde{E} \end{pmatrix}. \end{aligned} \quad (\text{B2})$$

Brundobler and Elser [32] found that elements of S-matrix for the time evolution given by Eq. (B1) can be approximated and expressed in terms of the transition probabilities p_{kl} between

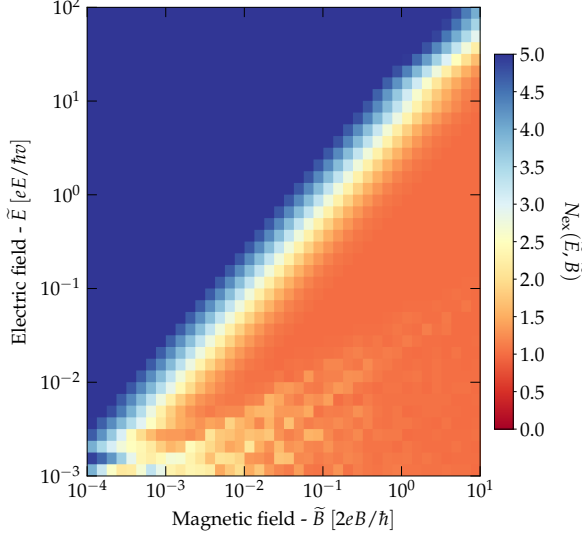


FIG. 10. The expectation value $N_{\text{ex}}(\tilde{E}, \tilde{B})$ of number of electrons in the conductive bands as a function of rescaled magnetic and electric fields - \tilde{B} and \tilde{E} for ideal Weyl Hamiltonian given by Eq. (A1).

the two states (of $\mathcal{H}(t)$) k and l only,

$$p_{kl} \approx e^{-\pi z_{kl}}, \quad (\text{B3})$$

where z_{kl} is the Landau-Zener parameter

$$z_{kl} = \frac{|\mathcal{A}_{kl}|^2}{|\mathcal{B}_{kk} - \mathcal{B}_{ll}|} \sim \tilde{B}/\tilde{E}. \quad (\text{B4})$$

Even though, we do not study the Landau-Zener problem of a single-electron Hamiltonian $\mathcal{H}(t)$, but rather a many-body Hamiltonian of its tensor product, it gives an insight, why only the ratio of electric and magnetic fields (fluxes) should influence the non-adiabatic corrections to $N_{\text{ex}}(\tilde{E}, \tilde{B})$ as demonstrated in Fig. 10.

For the calculation of $N_{\text{ex}}(\tilde{E}, \tilde{B})$, see Fig. 10, overall 13 LLs (after removal of one ghost state) were considered ($N = 7$), with up to $M = 5$ excited electrons yielding to overall 1709 Slater determinants and overall 283 k -points were used for the real-time dynamics simulation.

Appendix C: Calculation of dot product of two Slater determinants in $O(N^3)$

Here we show how the dot product of two Slater determinants can be calculated in $O(N^3)$ time. Considering two Slater

determinants

$$|\varphi_i\rangle = \frac{1}{\sqrt{N!}} \sum_{\tau} \text{sign } \tau \left(\otimes_k |\psi_{\tau(\alpha_i(k))}\rangle \right) \quad (\text{C1})$$

$$|\varphi'_j\rangle = \frac{1}{\sqrt{N!}} \sum_{\tau'} \text{sign } \tau' \left(\otimes_l |\psi'_{\tau'(\alpha_j(l))}\rangle \right), \quad (\text{C2})$$

we are interested into their dot product

$$\langle \varphi_i | \varphi'_j \rangle = \frac{1}{N!} \sum_{\tau'} \sum_{\tau} \text{sign } \tau' \text{sign } \tau \left(\prod_{k=1}^N \langle \psi_{i\tau(k)} | \psi'_{j\tau'(k)} \rangle \right). \quad (\text{C3})$$

Note that although the direct evaluation of the dot product requires $(N!)^2$ operations, there are just N^2 independent terms. Note also that the determinant of the matrix $M_{ij} = \langle \psi_i | \psi'_j \rangle$ can be expressed as

$$\det M \equiv \sum_{\tau'} \text{sign } \tau' \prod_{i=1}^N \langle \psi_i | \psi'_{\tau'(i)} \rangle, \quad (\text{C4})$$

where τ' is the corresponding permutation. Using $\det(AB) = \det A \cdot \det B$, one can see that matrix M permuted by τ has a determinant $\det(\tau M)$ equal to $\text{sign } \tau \det M$. On the other hand, $(\tau M)_{ij} = \langle \psi_{\tau(i)} | \psi'_j \rangle$, and thus it follows that

$$\begin{aligned} \det(\tau M) &\equiv \sum_{\tau'} \text{sign } \tau' \prod_{i=1}^N \langle \psi_{\tau(i)} | \psi'_{\tau'(i)} \rangle \\ &= \text{sign } \tau \det M. \end{aligned} \quad (\text{C5})$$

By multiplying both sides of the last equation by $\text{sign } \tau$ and summing over all $N!$ permutations covered by τ , we identify in $\det M$ the dot product of two Slater determinants $\langle \varphi_i | \varphi'_j \rangle$,

$$\langle \varphi_i | \varphi'_j \rangle = \det M. \quad (\text{C6})$$

We note that this formula was for the first time presented in Ref. [33].

Appendix D: Landau Levels of model non-symmorphic nodal loop Hamiltonian

In Figs. 11 - 13 we show the LLs of the model NSNL Hamiltonian - $\mathcal{H}_{\text{NSNL}}$ given by Eq. (15) as a function of the angle θ between the direction of the applied magnetic field and the plane of NSNL in the reciprocal space.

[1] N. P. Armitage, E. J. Mele, and A. Vishwanath, Weyl and dirac semimetals in three-dimensional solids, *Rev. Mod. Phys.* **90**,

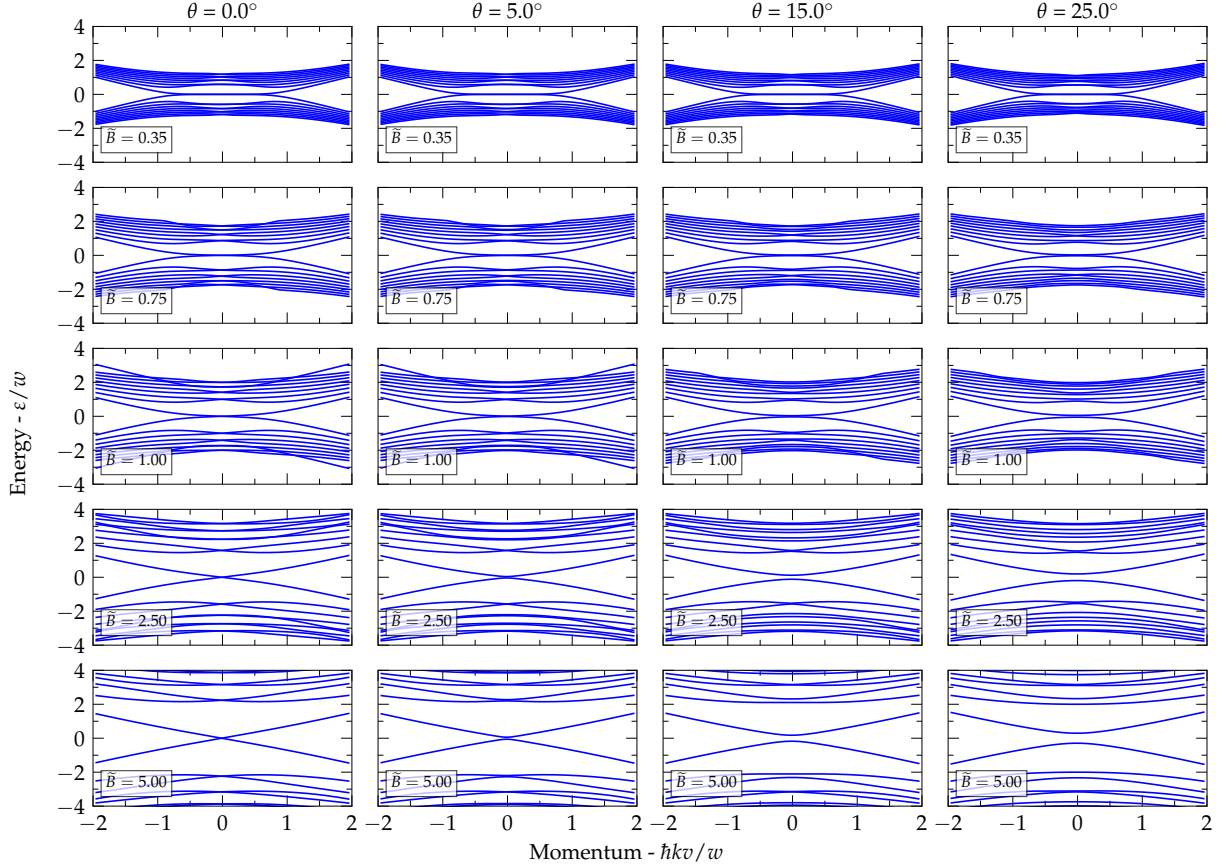


FIG. 11. LLs of $\mathcal{H}_{\text{NSNL}}$. Nine LLs below and above the Fermi level are shown.

- [2] B. Yan and C. Felser, Topological materials: Weyl semimetals, *Annual Review of Condensed Matter Physics* **8**, 337 (2017).
- [3] X. Wan, A. M. Turner, A. Vishwanath, and S. Y. Savrasov, Topological semimetal and fermi-arc surface states in the electronic structure of pyrochlore iridates, *Physical Review B* **83**, 10.1103/physrevb.83.205101 (2011).
- [4] C. Rylands, A. Parhizkar, A. A. Burkov, and V. Galitski, Chiral anomaly in interacting condensed matter systems, *Physical Review Letters* **126**, 10.1103/physrevlett.126.185303 (2021).
- [5] P. Hosur and X. Qi, Recent developments in transport phenomena in weyl semimetals, *Comptes Rendus Phys.* **14**, 857 (2013).
- [6] A. A. Zyuzin and A. A. Burkov, Topological response in weyl semimetals and the chiral anomaly, *Physical Review B* **86**, 10.1103/physrevb.86.115133 (2012).
- [7] D. T. Son and B. Z. Spivak, Chiral anomaly and classical negative magnetoresistance of weyl metals, *Phys. Rev. B* **88**, 104412 (2013).
- [8] H. B. Nielsen and M. Ninomiya, Absence of neutrinos on a lattice, *Nuc. Phys. B* **185**, 20–40 (1981).
- [9] P. E. C. Ashby and J. P. Carbotte, Magneto-optical conductivity of weyl semimetals, *Physical Review B* **87**, 10.1103/physrevb.87.245131 (2013).
- [10] H.-Z. Lu, S.-B. Zhang, and S.-Q. Shen, High-field magnetoconductivity of topological semimetals with short-range potential, *Physical Review B* **92**, 10.1103/physrevb.92.045203 (2015).
- [11] C. J. Tabert, J. P. Carbotte, and E. J. Nicol, Optical and transport properties in three-dimensional dirac and weyl semimetals, *Physical Review B* **93**, 10.1103/physrevb.93.085426 (2016).
- [12] C. J. Tabert and J. P. Carbotte, Optical conductivity of weyl semimetals and signatures of the gapped semimetal phase transition, *Physical Review B* **93**, 10.1103/physrevb.93.085442 (2016).
- [13] X. Dai, Z. Du, and H.-Z. Lu, Negative magnetoresistance without chiral anomaly in topological insulators, *Physical Review Letters* **119**, 10.1103/physrevlett.119.166601 (2017).
- [14] K. Das, S. K. Singh, and A. Agarwal, Chiral anomalies induced transport in Weyl metals in quantizing magnetic field, *Physical Review Research* **2**, 033511 (2020).
- [15] T. Bzdušek, Q. Wu, A. Rüegg, M. Sigrist, and A. A. Soluyanov, Nodal-chain metals, *Nature* **538**, 75 (2016).
- [16] K. Hwang, W.-R. Lee and K. Park, Electric quantum oscillations in Weyl semimetals, *Phys. Rev. Res.* **3**, 033132 (2021).
- [17] X.-Q. Sun, S.-C. Zhang, and T. Bzdušek, Conversion Rules for Weyl Points and Nodal Lines in Topological Media, *Phys. Rev. Lett.* **121**, 106402 (2018).

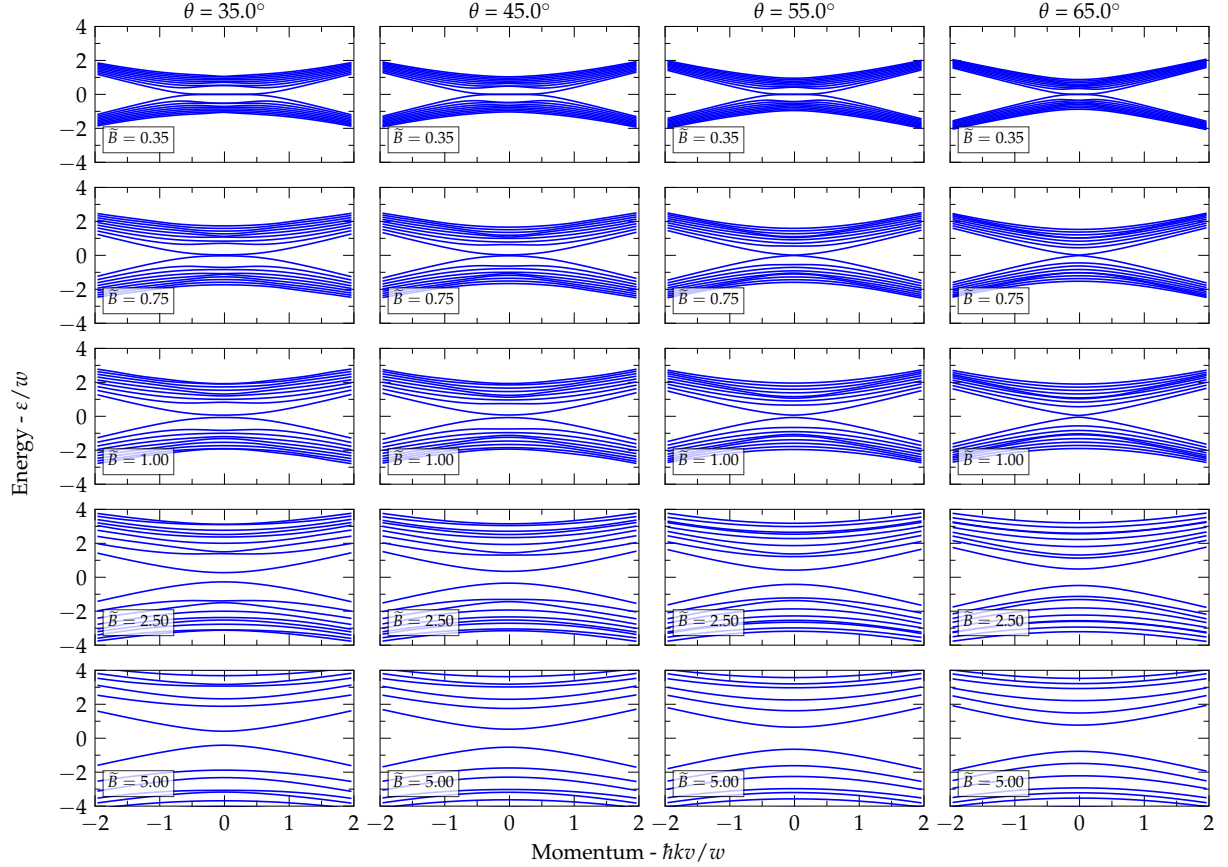


FIG. 12. LLs of $\mathcal{H}_{\text{NSNL}}$. Nine LLs below and above the Fermi level are shown.

- [18] A. Bouhon, Q. Wu, R.-J. Slager, H. Weng, O. V. Yazyev, and T. Bzdušek, Non-abelian reciprocal braiding of weyl points and its manifestation in ZrTe, *Nature Physics* **16**, 1137 (2020).
- [19] L.-K. Lim and R. Moessner, Pseudospin Vortex Ring with a Nodal Line in Three Dimensions, *Phys. Rev. Lett.* **118**, 016401 (2017).
- [20] G. Xu, H. Weng, Z. Wang, X. Dai, and Z. Fang, Chern Semimetal and the Quantized Anomalous Hall Effect in HgCr_2Se_4 , *Phys. Rev. Lett.* **107**, 186806 (2011).
- [21] A. Nelson, T. Neupert, A. Alexandradinata, and T. Bzdušek, Delicate topology protected by rotation symmetry: Crystalline hopf insulators and beyond, [arXiv:2111.09365v1](https://arxiv.org/abs/2111.09365).
- [22] Q. Wu, A. A. Soluyanov, and T. Bzdušek, Non-abelian band topology in noninteracting metals, *Science* **365**, 1273 (2019).
- [23] A. A. Soluyanov, D. Gresch, Z. Wang, Q.-S. Wu, M. Troyer, X. Dai, and B. A. Bernevig, Type-II Weyl semimetals, *Nature* **527**, 495 (2015).
- [24] B. Q. Lv, Z.-L. Feng, Q.-N. Xu, X. Gao, J.-Z. Ma, L.-Y. Kong, P. Richard, Y.-B. Huang, V. N. Strocov, C. Fang, H.-M. Weng, Y.-G. Shi, T. Qian, and H. Ding, Observation of three-component fermions in the topological semimetal molybdenum phosphide, *Nature* **546**, 627 (2017).
- [25] H. Weng, C. Fang, Z. Fang, B. A. Bernevig, and X. Dai, Weyl Semimetal Phase in Noncentrosymmetric Transition-Metal Monophosphides, *Phys. Rev. X* **5**, 011029 (2015).
- [26] B. Q. Lv, H. M. Weng, B. B. Fu, X. P. Wang, H. Miao, J. Ma, P. Richard, X. C. Huang, L. X. Zhao, G. F. Chen, Z. Fang, X. Dai, T. Qian, and H. Ding, Experimental Discovery of Weyl Semimetal TaAs, *Phys. Rev. X* **5**, 031013 (2015).
- [27] S.-Y. Xu, I. Belopolski, N. Alidoust, M. Neupane, G. Bian, C. Zhang, R. Sankar, G. Chang, Z. Yuan, C.-C. Lee, S.-M. Huang, H. Zheng, J. Ma, D. S. Sanchez, B. Wang, A. Bansil, F. Chou, P. P. Shibayev, H. Lin, S. Jia, and M. Z. Hasan, Discovery of a Weyl fermion semimetal and topological Fermi arcs, *Science* **349**, 613 (2015).
- [28] F. N. Ünal, A. Bouhon, and R.-J. Slager, Topological euler class as a dynamical observable in optical lattices, *Physical Review Letters* **125**, 10.1103/physrevlett.125.053601 (2020).
- [29] S. M. Young, S. Zaheer, J. C. Y. Teo, C. L. Kane, E. J. Mele, and A. M. Rappe, Dirac semimetal in Three Dimensions, *Phys. Rev. Lett.* **108**, 140405 (2012).
- [30] B.-J. Yang and N. Nagaosa, Classification of stable three-dimensional Dirac semimetals with nontrivial topology, *Nat. Commun.* **5**, 4898 (2014).

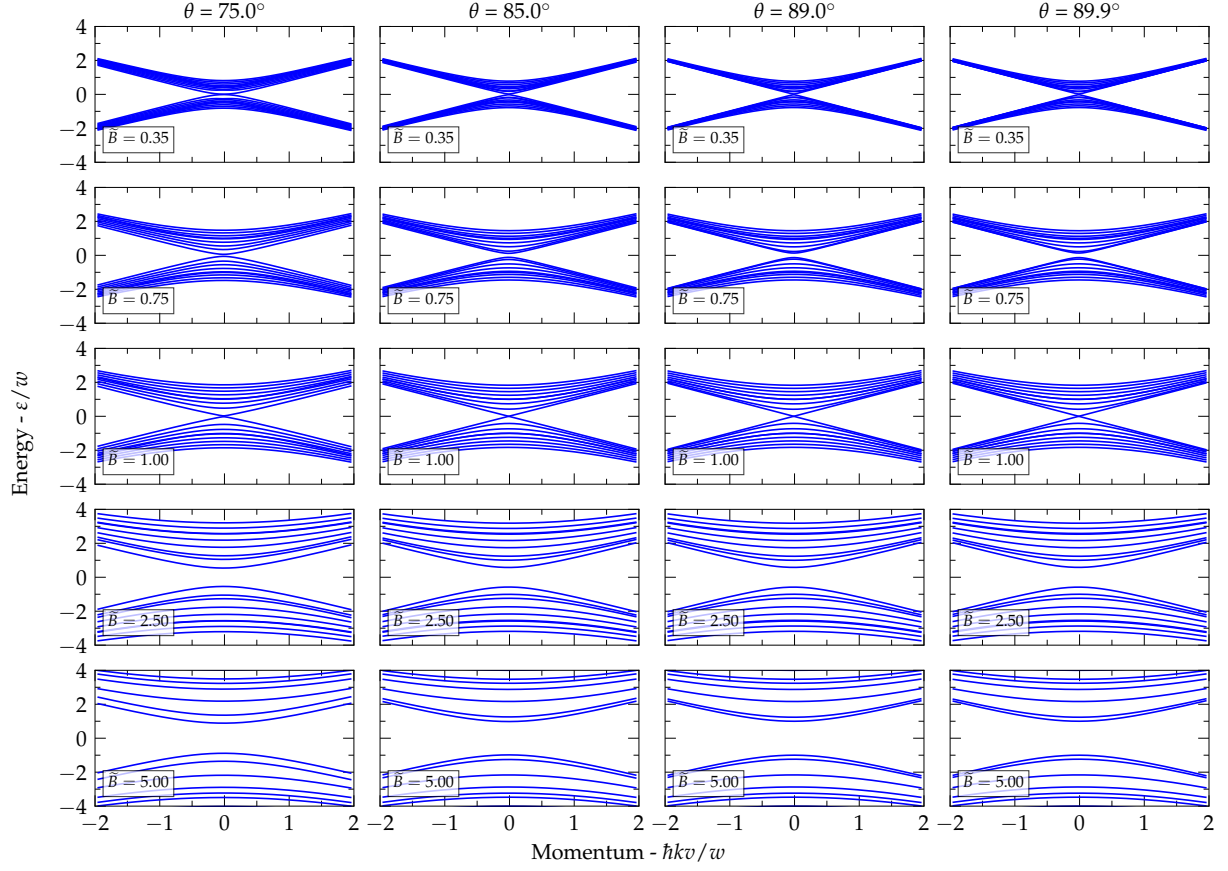


FIG. 13. LLs of $\mathcal{H}_{\text{NSNL}}$. Nine LLs below and above the Fermi level are shown.

- [31] B. J. Wieder, Y. Kim, A. Rappe, and C. Kane, Double dirac semimetals in three dimensions, *Physical Review Letters* **116**, 10.1103/physrevlett.116.186402 (2016).
- [32] S. Brundobler and V. Elser, S-matrix for generalized landau-zener problem, *Journal of Physics A: Mathematical and General*

- 26**, 1211 (1993).
- [33] P.-O. Löwdin, Quantum theory of many-particle systems. i. physical interpretations by means of density matrices, natural spin-orbitals, and convergence problems in the method of configurational interaction, *Physical Review* **97**, 1474 (1955).